Human-on-leaf-chip: A biomimetic vascular system integrated with chamber-specific organs

Mao Mao[1,2], Ho Pan Bei[1], Chun Hei Lam[1], Pengyu Chen[2], Shuqi Wang[3,4], Ying Chen[5], Jiankang He[2], Xin Zhao[1]**

[1] Department of Biomedical Engineering, The Hong Kong Polytechnic University, Hung Hom, Hong Kong, China

[2] State Key Laboratory for Manufacturing Systems Engineering, Xi'an Jiaotong University, Xi'an, 710049, China

[3] State Key Laboratory for Diagnosis and Treatment of Infectious Diseases, National Clinical Research Center for Infectious Diseases, National Medical Center for Infectious Diseases, Collaborative Innovation Center for Diagnosis and Treatment of Infectious Diseases, The First Affiliated Hospital, College of Medicine, Zhejiang University, Hangzhou 310003, Zhejiang, China

[4] Institute for Translational Medicine, Zhejiang University, Hangzhou 310029, Zhejiang, China

[5] Guangdong Provincial Key Laboratory of Functional Soft Condensed Matter, School of Materials and Energy, Guangdong University of Technology, Guangzhou 510000, Guangdong, China

Email: jiankanghe@mail.xjtu.edu.cn; xin.zhao@polyu.edu.hk

Keywords: organ on a chip, microfluidics, vasculature, cancer metastasis

Abstract

Vascular network is a central component of organ-on-a-chip system to build a three-dimensional (3D) physiological microenvironment with controlled physical and biochemical variables. Inspired by ubiquitous biological systems such as leaf venation and circulatory systems, a fabrication strategy is devised to develop a biomimetic vascular system integrated with freely-designed chambers, which function as niches for the chamber-specific vascularized organs. As a

proof of concept study, human-on-leaf-chip system with a biomimetic multiscale vasculature system connecting the self-assembled 3D vasculatures in chambers is fabricated, mimicking the *in-vivo* complex architectures of the human cardiovascular system connecting the vascularized organs. Besides, two types of vascularized organs are built independently within the two halves of the system to verify its feasibility for conducting a comparative experiment for organ-specific metastasis study in a single chip. Successful culturing of HepG2s and mesenchymal stem cells (MSCs) with HUVECs shows good vasculature formation, and organ-specific metastasis is simulated through perfusion of pancreatic cancer cells and shows distinct cancer encapsulation by MSCs absent in HepG2s. Given the good culture efficacy, study design flexibility and ease of modification, these results show that our bioinspired human-on-leaf-chip possesses great potential in comparative and metastasis studies while retaining organ-to-organ crosstalk.

Introduction

Noteworthy efforts have been devoted to creating organ-on-a-chip systems for culturing living cells in perfused, miniaturized platforms in order to satisfy the urgent needs of establishing physiologically-functional tissues or organs as *in-vitro* disease models for drug screening and disease pathology studies.[1-3] To remedy the limitations of conventional two-dimensional (2D) or three-dimensional (3D) culture systems such as a lack of supportive vasculature formation and inability to accommodate biomimetic dynamic cultures, organ-on-chips are expected to recapitulate the *in-vivo* 3D tissue multiscale architecture and the complex organ-specific biophysical and biochemical microenvironments.[4, 5] Vasculature is essential for interconnection between organs and serves as a semi-permeable barrier to dynamically regulate the exchange of molecules and cells between the flowing fluids and surrounding tissue, closely related to some

critical diseases such as metastasis and inflammatory diseases.[6-8]

Numerous approaches have been developed over the past decades to incorporate hollow, perfusable microchannels to represent human vasculature within various types of 3D biomaterial [e.g. polydimethylsiloxane (PDMS), hydrogel] on chips[9, 10] such as simple needle templating[11], sacrificial molding[12] and microreplication-based layer-by-layer assembly[13]. It is found that the vessel geometry and flow characteristics had a noticeable effect on the endothelium-related biological functions and activities.[14, 15] However, most of the existing models are limited to completely straight channels of more than 50 μm in diameter, significantly differing from the blood vessels found in mammalian cardiovascular and respiratory systems, which are usually arranged in hierarchical structures made up of interconnections and bifurcations with vessels whose diameters vary dramatically.[3, 6] Moreover, those artificially-created channels differ greatly from natural vasculature system in terms of energy efficiency and fluid flow, and lack the signaling between organs through a biologically assembled endothelial lining.

Thus considerable attention has been directed towards engineering vascular system on chips inspired by the natural complex vascular networks, through which animals and plants transport fluids and cells efficiently over a long distance.[16, 17] Many breakthroughs have been made to establish a set of biomimetic design principles to achieve physiologic blood flow within an artificial vascular network.[18] Murray's law, originally obtained from the study of mammalian cardiovascular systems describing the optimum conditions of the branching hierarchical structures of blood vessels, has been broadly utilized to design artificial vascular microfluidic networks.[19] While mammalian cardiovascular networks may prove to be difficult to extract or recapitulate due to their complex morphology and diverse sizes, leaf venation network, another pervasive nature-selected hierarchical yet simple, bifurcating channels to transport fluids

efficiently, was also proven to obey Murray's law.[20] With consideration of the remarkable similarities between leaf venation and mammalian blood vessel regarding the vascular architecture and high-efficient transportation function, researchers began to use the leaf venation network to engineer biomimetic vascular networks on chips.[21-24] Although these strategies were able to fabricate the leaf-venation-inspired microfluidic channels into various types of materials, none of them allowed for the modification of networks for stable chambers in the direct templating process, leading to the failure of integration of multiple functional organs into those chip systems. Notably, leaf venation networks are resistant to damage in that they are composed of hierarchically nested loops, hence fluid can reach all parts of a damaged leaf. This feature supports integration of chambers into the leaf-venation-inspired microfluidic channels while maintaining their optimized flow.[25] Also, the architecture of leaf venation can be considered bilaterally symmetrical along the main channels, which provides us with more inspiration for biomimetic designs and applications.

To mimic the *in-vivo* conditions of the vital organs connected by the hierarchic cardiovascular system while capturing the advantage of innate leaf symmetry and allowing for flexible modifications, we propose here a novel biomimetic vascular system integrated with freely-designed chambers, which function as niches for the chamber-specific vascularized organs (**Figure 1a**). Inspired by previous microfluidic studies of leaf venation resemblance to human vasculature systems and to achieve perfused co-culture of various organs for research and screening purposes, we digitalized the leaf venation design of Osmanthus Fragrans as a CAD file to accommodate chambers for multi-organ culture, and transferred said design to PDMS for a high-throughput, one-way and modifiable human-on-leaf-chip. Experimental perfusion study demonstrated independent fluid flowing in half-and-half mode along the main vein within our

biomimetic vascular system, and the existence of organs has an insignificant effect on flow velocity distribution within the microfluidic channels, which was further supported by the result of computational fluid dynamics analysis. As proof of concept study, the biomimetic vascular channels were endothelialized to link the self-assembled 3D vasculature between chambers, showing the potential to fabricate a human-on-leaf-chip with vascularized organs, mimicking the complex architectures of the human cardiovascular system that connected the organs (**Figure 1b(i)**). Besides, vascularized liver and bone organs representing soft and hard tissues respectively were fabricated within the biomimetic vascular system to verify its feasibility for organ-specific metastasis study (**Figure 1b(ii)**).

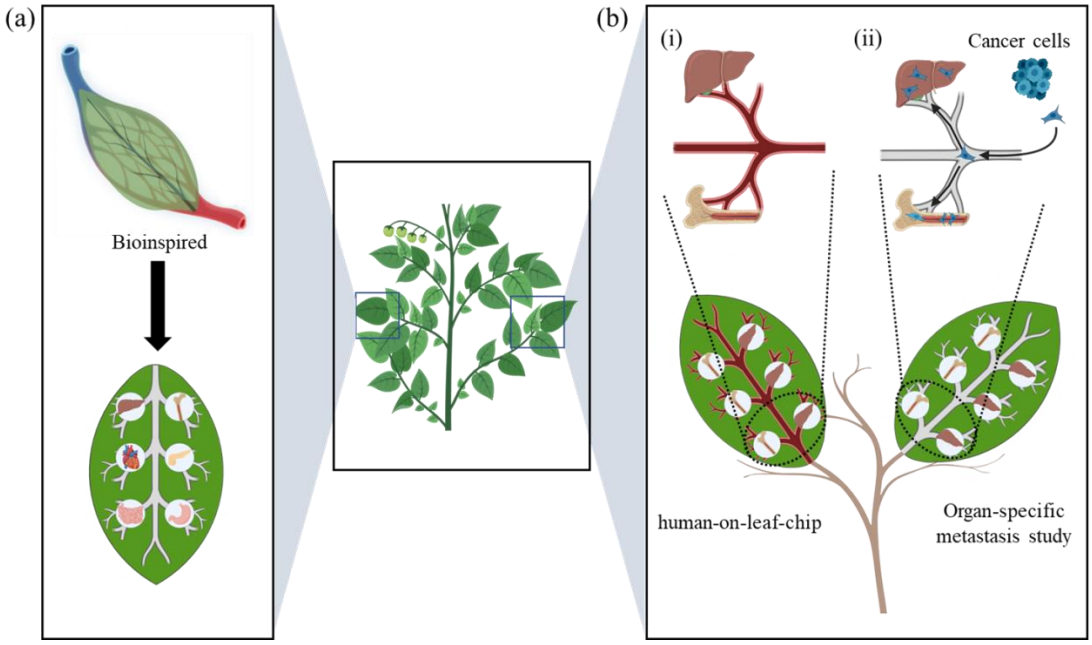

Figure 1. Biomimetic design of a vascular system integrated with chamber-specific organs. (a) Schematic diagram of a leaf-venation-based biomimetic vascular system integrated with organs. Credit: The Ready Campaign, Community Emergency Response Team. (b) As proof-of-concept studies, the system can be employed to build human-on-leaf-chip (i) and to study organ-specific metastasis (ii). Illustration created with Biorender.

Result and discussion

1. Design and fabrication of the biomimetic vascular system with integrated chambers

The aim of this work is to develop a biomimetic vascular system to support the perfused culture of vascularized organs. The biomimetic vascular system mainly consisted of a PDMS layer with biomimetic vascular networks and integrated chambers sandwiched by two poly(methyl methacrylate) (PMMA) sheets to create a sealed perfusable microenvironment (**Figure 2a**). Holes were produced in the PDMS layer and PMMA sheets to work as inlet and outlet, which were connected by Teflon tubes to syringes driven by a syringe pump. Before assembly of the chip, cells/hydrogel were seeded into the chambers, which functioned as living niches for the organs. Flowing medium was expected to perfuse through the entire biomimetic vascular networks and diffuse throughout the 3D hydrogel to maintain the mass transport in encapsulated cells.

Figure 2b shows the main procedures to fabricate the biomimetic vascular system integrated with freely-designed chambers. The CAD file of the leaf venation network with hierarchical bifurcating architectures was acquired from the high-quality photo of leaf venation skeleton via a series of image processing steps. This file could be edited freely using the commercial software AutoCAD, where 2 mm diameter chambers and inlet/outlet were added. Specifically, two inlets and one outlet were added at the beginning and end of the main vein respectively. The edited pattern was then used to fabricate a photomask for etching the silicon wafer, which was further molded to obtain the PDMS layer with the biomimetic vascular networks connecting the integrated chambers (**Figure S1**). **Figure 1c** is a photograph of the final assembled biomimetic vascular system. Red ink was perfused throughout the biomimetic

vascular system, demonstrating the interconnection of the biomimetic vascular channels and the integrated chambers (**Figure 2d**). Representative microscopical image shows that the red dye only exists in the biomimetic vascular channels and the integrated chambers, indicating that no leakage occurs between the PDMS layer and the PMMA sheet.

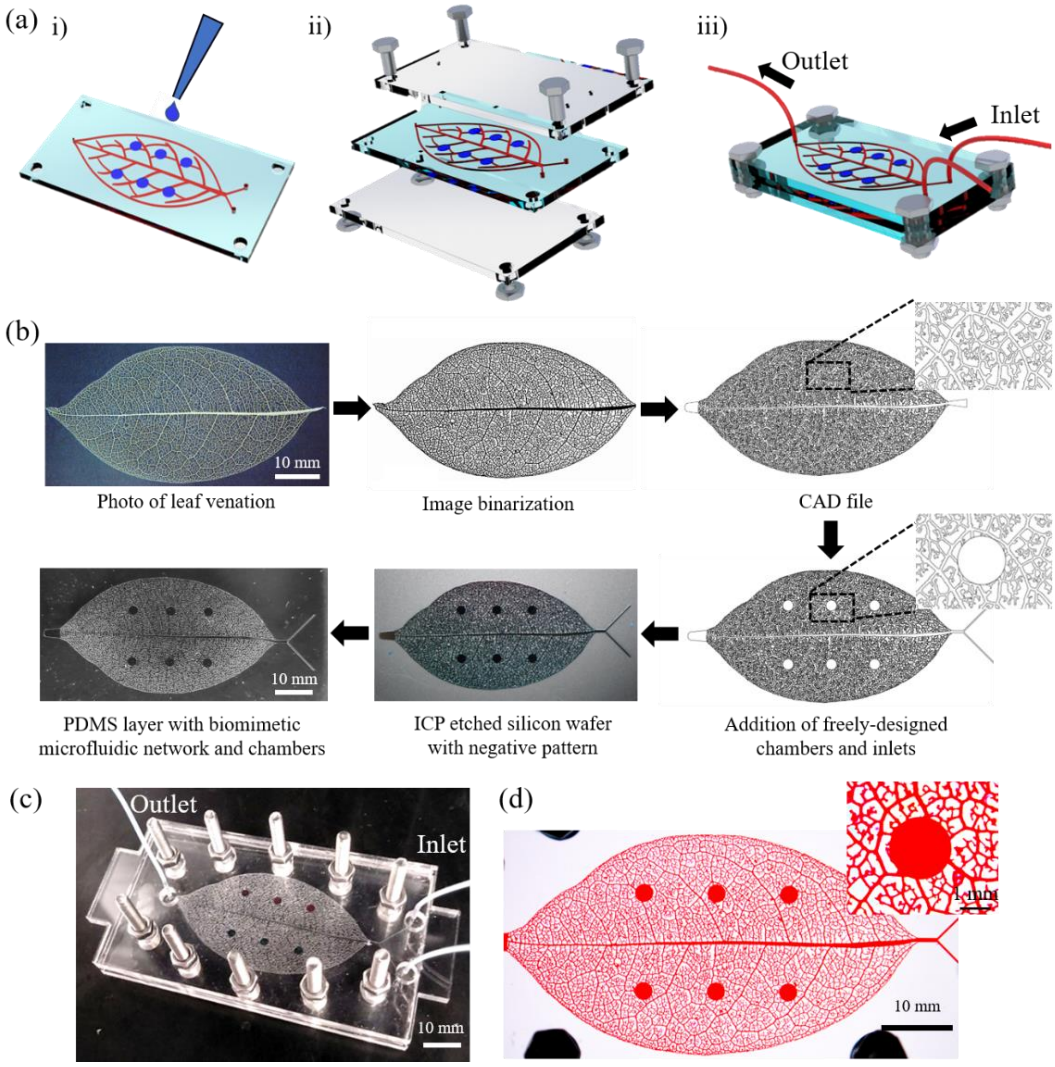

Figure 2. Fabrication of the biomimetic vascular system with integrated chambers. (a) Schematic diagram of the biomimetic vascular system, consisting of two PMMA sheets and a PDMS layer with the biomimetic vascular network. The chambers are seeded with cells/hydrogel before assembling. (b) Fabrication process from leaf venation skeleton to biomimetic vascular network

integrated with freely-designed chambers in the PDMS layer. (c) Photograph of the assembled biomimetic vascular system. (d) Interconnected biomimetic vascular networks and chambers suffused with red ink.

Many approaches have been developed to fabricate microfluidic chips with the biomimetic vascular networks of leaf venation, such as using leaf venation skeleton as a photo-mask for microfabrication [24] or direct replicating mold [26], as well as using decellularized leaf as cell seeding scaffolds [27], demonstrating the potential of leaf-venation-inspired microfluidic networks for engineering vascularized tissues on chips. However, none of these approaches allow for modification of the vascular networks of leaf venation, which makes it impossible to integrate living niches for culturing various organs. To overcome this problem, our novel strategy here employs the CAD file of leaf venation network, obtained by series of image processes, to fabricate a photo-mask for following mold-etching, which supports the free addition of predesigned chambers with any size in any position due to the leaf's unique niche of laminar flow even with defects.

2. Fluid transport in half-and-half mode within the biomimetic vascular system

One basic function of leaf venation is to transport water to the surrounding tissues in leaf, which is thought to undergo a process of gradual optimization through evolution.[28] Thus the fluid transfer within the leaf venation networks was investigated, showing its merits like maximizd water flow rate and minimized water pressure drop caused by the water flow, which culminated in governing architectural principles such as Murray's law.[20, 29] It was also found that the multiscale microfluidic network of leaf venation within the agarose matrix was capable of

transporting fluid sufficiently and rapidly without the assistance of external pumps, regardless of whether the microfluidic chip was placed at any positive or negative inclination angles.[30] More investigations are thus encouraged, which might give us the inspiration to design network-matrix architectures and merit for a variety of practical applications.

Since the architecture of leaf venation can be roughly considered as bilaterally symmetrical along the main channels, ink perfusion was conducted to investigate whether the flow transfer would also have the corresponding symmetry within our system. After complete suffusion with pure water, the biomimetic vascular system was perfused with water and blue ink through the two inlets independently at the same speed of 50 μL/min. The blue ink took approximately 30s to fully perfuse one half of the biomimetic vascular system, during which a clear boundary formed and was maintained between the flowing water and blue ink, indicating they were in a stable laminar flow along the main channels (**Figure 3a**). Afterwards, the inlet perfused by water was changed to be perfused by red ink, which also took approximately 30 s to suffuse the other half, further confirming the interesting phenomenon of perfusion in half-and-half mode within the biomimetic vascular system. The perfused areas by the blue and red ink every 3 s were calculated and normalized by the corresponding half of the biomimetic vascular system. The curve of the perfusion ratio was nearly symmetrical, demonstrating that the velocity of the flow transfer might be identical within both halves of the biomimetic vascular system (**Figure 3b**). **Figure 3c** shows that the inks could also perfuse throughout the whole biomimetic vascular system with six chambers using approximately 30 s, which were pre-filled with fibrin hydrogel to mimic the subsequent cell culture condition. The microscopical image clearly indicated that the existence of chambers had no effect on the half-and-half perfusion along the main vein (**Figure 3d, Figure S2**). In short, two independent flowing fluids in half-and-half mode could be achieved within our

biomimetic vascular system, regardless of whether there are integrated chambers, indicating the possibility to conduct comparative experiments by culturing two independent troops of organs in the chambers along the two sides.

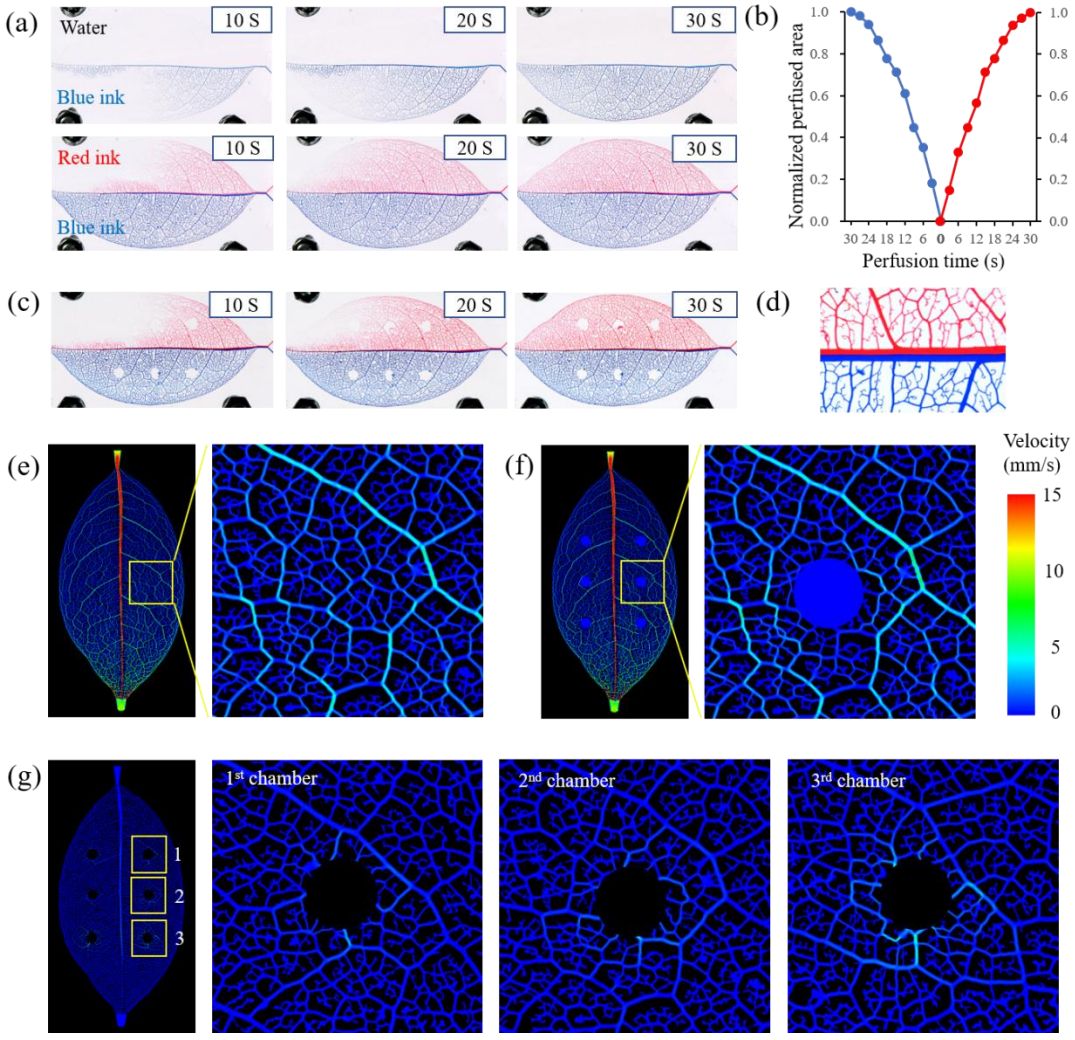

Figure 3. Fluid transport within the biomimetic vascular system. (a) Representative images of the ink-perfused biomimetic vascular system with no chamber at different time points, showing half-and-half perfusion along the main vein. (b) The ratio of the perfused area by blue and red dye at different time points. (c) Representative images of ink-perfused biomimetic vascular system integrated with six chambers filled with fibrin hydrogel at different time points, showing half-and-half perfusion along the main vein. (d) Microscopical image showing half-red and half-

blue within the main vein. Computational simulation of flow velocity vectors in the biomimetic vascular system with no chamber (e) and six chambers (f). (g) Computational study of the change of flow velocity within the biomimetic vascular networks caused by the six chambers. The contours show the difference of flow velocity within the biomimetic vascular networks beyond the chambers between (e) and (f).

3. Modeling of fluid transport within the biomimetic vascular network with chambers

To further investigate the effect of chambers on flow transfer within the biomimetic vascular network theoretically, we perform a numerical finite-element simulation model based on ANSYS Fluent. The chambers are considered as porous zones to simulate the seeded hydrogel in chambers for 3D cell culture, while the biomimetic vascular network is set to be the fluid zone. The flow inside the microfluidic channels is assumed as a steady, incompressible laminar flow. The simulation parameters are shown as follow: The dynamic viscosity and density of flow medium are 1.005×10^{-3} Pa·s and 1000 kg/m^3 respectively; The porosity and viscous resistance of the porous zone are 0.99 and 6.667×10^{12} m^{-2}; The velocity of inlet and the gauge pressure of outlet are set as 9.024 mm/s and 0. **Figure 3e and 3f** show the distribution of flow velocity within the biomimetic vascular system with 0 and 6 chambers respectively, indicating no significant difference between them. To more clearly show the change of flow velocity field within the biomimetic vascular system induced by the introduction of 6 chambers, these two cases processed by ANSYS Fluent were then imported into the software Ansys Ensight and processed using the CasemapDiff Calculator function, which was able to compare a variable across cases. After calculation, we could obtain the contours showing the difference of flow velocity within the biomimetic vascular networks between Figure 3e and 3f (**Figure 3h**). It can

be found that the change of flow velocity only exists within the channels in a small zone near the chambers, suggesting that the introduction of chambers has little effect on flow velocity within the biomimetic vascular system. This result could help to validate the result of perfusion experiments that the chambers have an insignificant effect on perfusion time and half-and-half perfusion within the biomimetic vascular system. This interesting characteristic of the biomimetic vascular network might be owing to its hierarchic networks with a large number of closed loops, which was found in previous research work that the vascular redundancy in the leaf venation system contributes strongly to the tolerance of vein damage for transporting fluid.[25, 31]

4. Characterization of FITC-dextran diffusion within the chambers pre-seeded with fibrin hydrogel

To evaluate the nutrition supply for perfusion co-culture of cells within the chambers pre-seeded with fibrin hydrogel through the biomimetic vascular networks, FITC-dextran solution was perfused as the simulation of culture media and its diffusion within the chambers was quantified. **Figure 4a** shows the representative images of FITC-dextran distributed in a chamber at different perfusion times and the corresponding fluorescent intensity along the measured baseline. It was found that the FITC-dextran could gradually diffuse from the empty microfluidic channels into the hydrogel within the chambers with the increase of perfusion time. The fluorescence intensity decreased along the direction of flow during the perfusion process, demonstrating that the flow from the channels may also contribute to FITC-dextran's permeation in the chamber through pressure-driven convections. After one hour's perfusion, there was no significant statistical difference in the average fluorescence intensity among the different chambers, indicating that the biomimetic vascular networks were able to provide sufficient nutrition to the cells encapsulated

in 3D hydrogel within all the six chambers (**Figure 4b**).

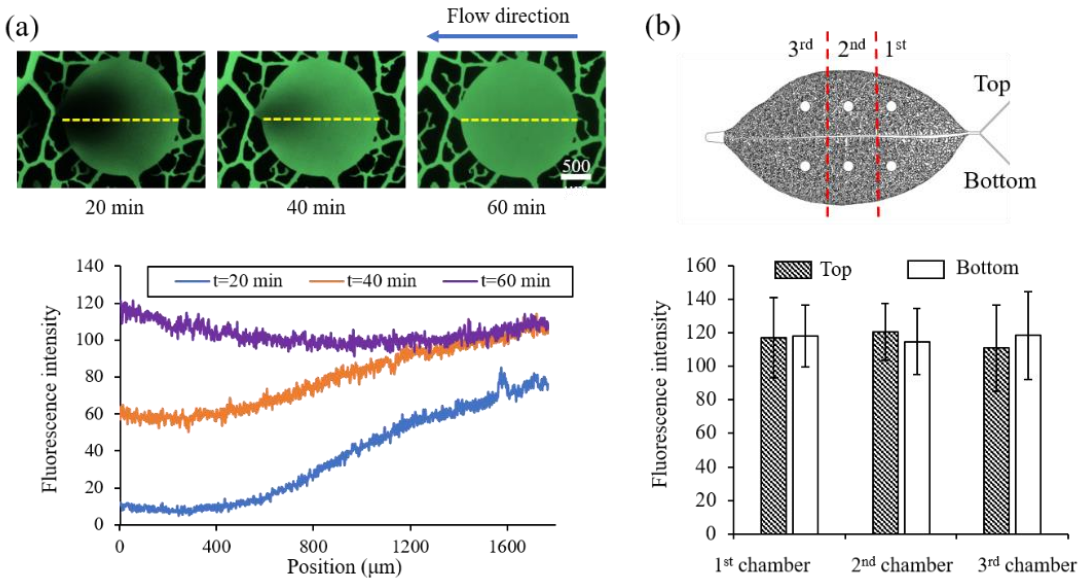

Figure 4. Characterization of FITC-dextran diffusion within the chambers pre-seeded with fibrin hydrogel. (a) Representative fluorescence images of the diffused FITC-dextran from empty channels into a fibrin-hydrogel-filled chamber at different time points and the corresponding temporal diffusion profile of FITC-dextran along the measured baseline. (b) The average fluorescence intensity in the different chambers after one hour's perfusion (statistical significance<0.01). cardiovascular system connecting the vascularized organs.

5. A proof-of-concept human-on-leaf-chip system with biomimetic vasculature connecting vascularized organs

We next sought to use the biomimetic vascular system to build 3D vascularized organs within chambers. Fibrin hydrogel encapsulated with human umbilical vein endothelial cells (HUVECs) was seeded into the chambers for perfused culture. At the beginning 2 days of culture, the HUVECs began to elongate and connect with each other. After 4 days of culture, they self-assembled into a 3D branched microvascular network enclosed in the fibrin hydrogel (**Figure**

5a). Fluorescent live/dead assay showed high viability of HUVECs within the chambers, indicating sufficient mass transfer provided by the biomimetic vascular channels (**Figure 5b**). F-actin staining was further conducted to clearly show the 3D capillary bed morphology and calculate the sizes of the vasculature within the chambers (**Figure 5c, d and Figure S3a**). The cross-sectional view showed the formation of lumen structures. Quantitative results indicated that there was no statistically significant difference in the projected microvasculature area among the six chambers, demonstrating that the biomimetic vascular system was able to provide comparable 3D living microenvironment for the cells/hydrogel in the integrated chambers (**Figure S3b**).

Inspired by the vital organs in the human body connected by the hierarchic cardiovascular system to provide perfused blood, we attempt to build a human-on-leaf-chip system by endothelializing the biomimetic vascular networks to connect the self-assembled 3D vasculature in the chambers. To distinguish the HUVECs within different locations of the chips, we labeled the HUVECs with green and red cell trackers respectively before cell seeding. The chip was assembled after seeding green HUVECs/ fibrin hydrogel into the chambers. Red HUVEC suspension in culture medium was then seeded into the biomimetic vascular networks by multiple perfusion-seeding, which finally lined the entire networks including the junctions between vessels of differing diameters and small ending channels. Under the constant flowing condition, HUVECs' orientations aligned with the direction of flow in the channels (**Figure S3c**). **Figure 5e** is the stitched image indicating that the green self-assembled vasculatures within the integrated chambers were well connected with the red endothelialized biomimetic vascular networks with complex hierarchical architectures. Figure 5f and 5g are the 3D view and cross-sectional view of the regional endothelialized biomimetic vascular networks, demonstrating that

the endothelial cells reached confluence and covered the 3D inner surface of the channels under perfusion condition, while **Figure 5h and 5i** show the integration of red endothelialized biomimetic vascular networks and the green 3D self-assembled vasculatures. These results illustrate the potential of our strategy to fabricate a human-on-leaf-chip system with a biomimetic perfusable vasculature connecting the integrated vascularized organs, mimicking the *in-vivo* complex architectures of the human cardiovascular system connecting the vascularized organs.

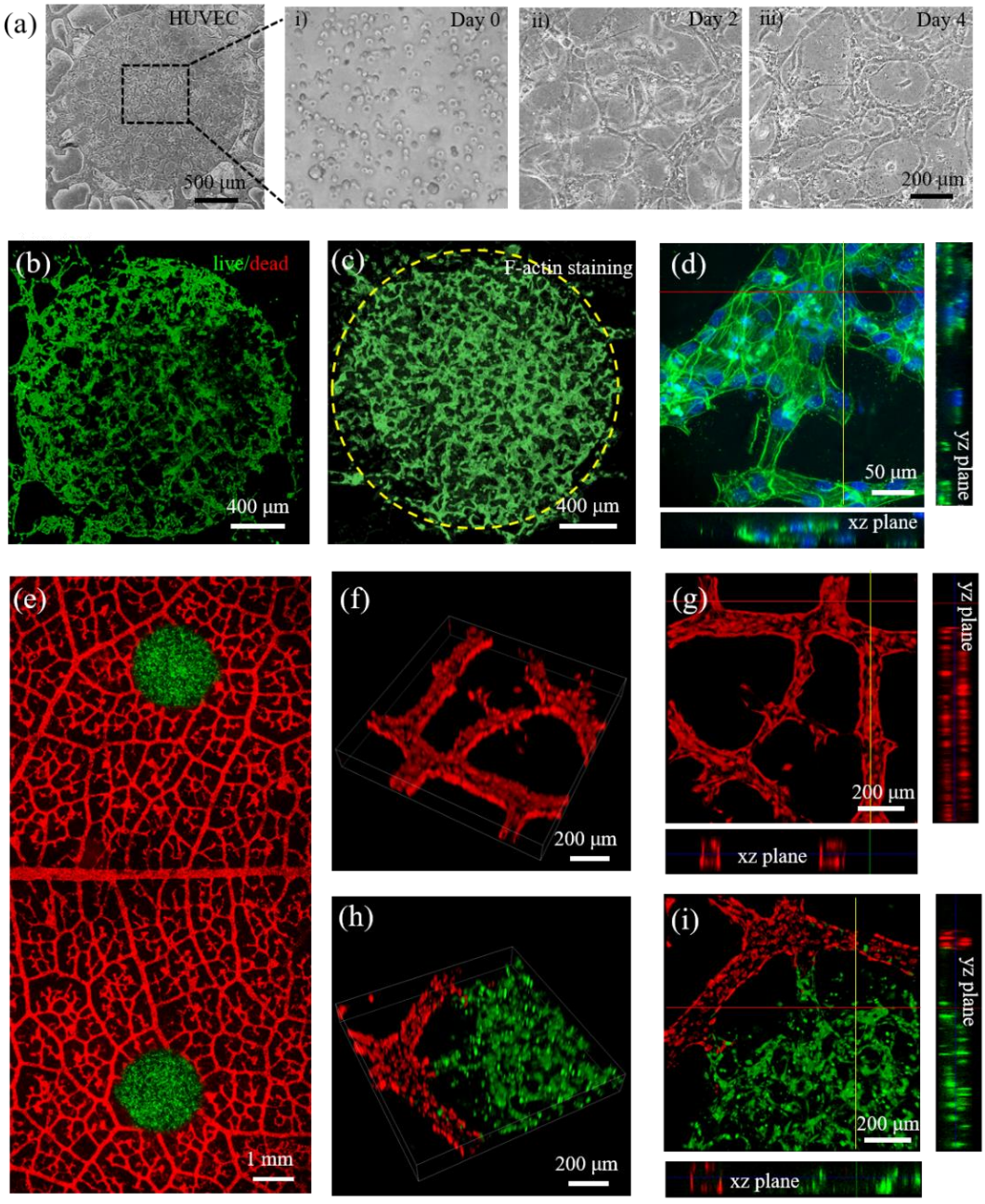

Figure 5. Endothelialization of the biomimetic vascular networks to connect vascularized organs. (a) Phase-contrast images of HUVECs forming microvasculature in a chamber over 4 days of culture. (b) Viability of the self-assembled microvasculature in a chamber. (c) F-actin staining showing the morphology of the self-assembled microvasculature in a chamber. (e) Cross-sectional view demonstrating the hollow lumen of the vessels. (e) The stitched

fluorescence image of the endothelialized biomimetic vascular networks (red) connecting the self-assembled microvasculatures (green) in chambers. (f, g) 3D view and cross-sectional view demonstrating hollow lumen of the endothelialized microfluidic channels. (h, i) The conjunction of endothelialized microfluidic channels (red) and the self-assembled microvasculature (green).

6. The biomimetic vascular system with multiple types of vascularized organs for organ-specific pancreatic metastasis study.

As an illustrative demonstration, we further built two types of vascularized organs within our biomimetic vascular system and did a comparative experiment for organ-specific metastasis study in a single chip. Metastasis, which involves disseminated cancer cells from the primary tumor site and initiating new tumors at distant organ sites by circulation and repeated crossing through the blood vessel system, is the main cause of cancer-related deaths.[32] It has been found that the primary cancer cells tend to converge to other specific organs more predominantly (e.g., colorectal cancer usually to liver).[33, 34] Organ-on-chip technology, while allowing for spatial and temporal control of cell growth and stimuli with microfluidic channels, also creates new opportunities for the study of metastasis with biomimetic complex biochemistries and geometries of the extracellular matrix.[35]

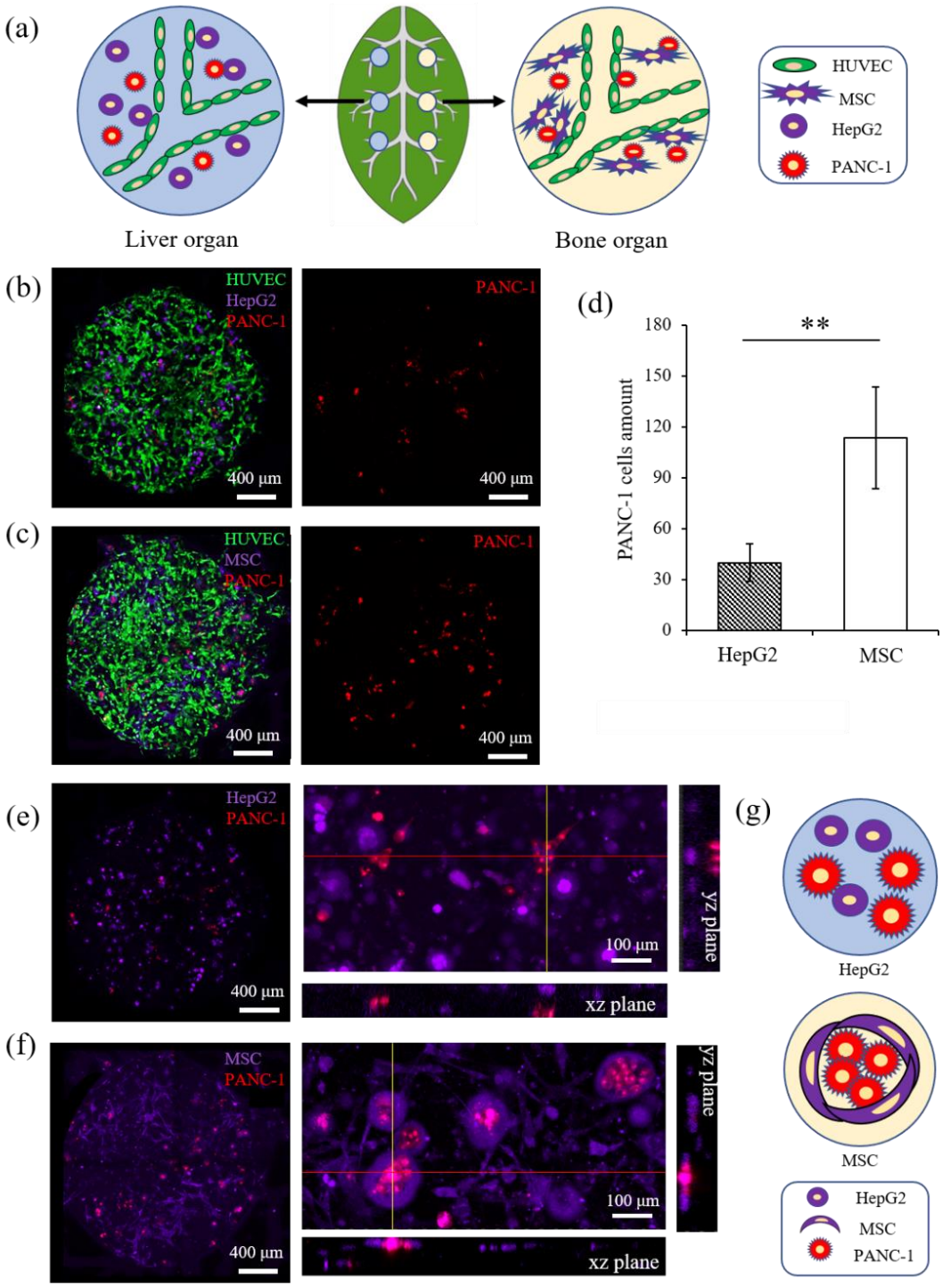

Figure 6. Perfused culture of vascularized organs in the biomimetic vascular system for studying organ-specific pancreatic cancer metastasis. (a) Schematic diagram of vascularized liver organs and vascularized bone organs in the biomimetic vascular system, metastasized by PANC-1

cancer cells. Representative confocal images (b,c) and quantitative statistics analysis (d) of PANC-1 cancer cells (red) in vascularized liver organs and vascularized bone organs exposed to perfused flow at day 6. (e,f) Projected overall view of the entire chambers and cross-sectional view demonstrating the position relationship between HepG2 cells (violet) and PANC-1 cancer cells (red), as well as MSCs (violet) and PANC-1 cancer cells (red). (g) Schematic diagram demonstrating the position relationship between HepG2 cells and PANC-1 cancer cells, as well as MSCs and PANC-1 cancer cells.

Since our biomimetic vascular system supports two independent flowing fluids in half-and-half mode along the main channels and the formation of 3D vasculature in the chambers, we sought to culture two independent troops of organs, including the vascularized bone organs (representing hard tissues) and liver organs (representing soft tissues) in the chambers along the two sides of the biomimetic vascular system for studying the organ-specific metastasis of pancreatic cancer (**Figure 6a**). The mixture of primary HUVECs labeled with green cell tracker and HepG2 cells labeled with violet cell tracker or primary MSCs labeled with violet cell tracker were embedded in fibrin hydrogel and seeded into the chambers within the two halves of the biomimetic vascular system respectively, to generate vascularized liver organs and bone organs. After 4 days of dynamic culture, functional vascularized organs were formed within the chambers, and the pancreatic cancer cells (PANC-1) labeled with red cell tracker were introduced and cultured for another 2 days. Afterwards, the metastatic colonization of the red cancer cells could be found within both organs (**Figure 6b and 6c**). The extravasated number of the cancer cells in the bone organs was significantly higher compared with the liver organs (**Figure 6d**). This result indicated that the vascularized MSC-microenvironment might provide a

preferable platform for the growth of pancreatic cancer cells. This is in accordance with previous studies which reported that MSCs preferentially accumulate to pancreatic cancers *in-vivo* to promote tumor growth, metastasis and angiogenesis.[36, 37] We also observed a very interesting phenomenon that some of the red PANC-1 cancer cells were encircled by the violet MSCs which situation did not occur between PANC-1 cancer cells and HepG2 cells in the liver organs (**Figure 6e and 6f**). **Figure 6g** is a schematic to clearly show the spatial position relationship of the cells within the organs. Pancreatic cancer is among the most lethal cancers in part owing to its aggressive metastatic nature. The development of 3D organotypic *in-vitro* microfluidic models to study the specificity of pancreatic cancer cells is important to improve the understanding of the mechanistic determinants of metastatic colonization underlying the metastatic process for better prevention and treatment of metastatic cancer. To the best of our knowledge, this is the first time to observe the spatial position relationship within 3D hydrogel between extravasated pancreatic cancer cells and MSCs, suggesting some biological mutual cellular interaction which still needs further investigation.

Conclusion

In summary, a novel strategy was proposed to fabricate a biomimetic vascular system integrated with chamber-specific vascularized organs. Through series of image processes, the CAD file of the leaf venation network was obtained, which enabled the predesigned addition of chambers with any size in any position and could be employed to fabricate the photo-mask for the following mold-etching. It was found that the final assembled chip could be perfused by two independent flowing fluids in half-and-half mode along the main vein regardless of chamber presence with an insignificant effect on flow velocity distribution within our system. These

characteristics might be owing to the bilaterally symmetrical and reticulate, hierarchical architectures of leaf venation networks. As an illustrative demonstration, two types of vascularized organs were built within the chambers located in two halves of the biomimetic vascular system respectively, which were then proven to enable the comparative experiment on a single chip for organ-specific metastasis study. The system also allowed for the confluent endothelialization of the inner surface of channels to build biomimetic perfusable vasculature system connecting the self-assembled 3D vasculature in the chambers, giving us new insights into engineering a human-on-leaf-chip system, mimicking the *in-vivo* complex architectures of the human cardiovascular system connecting the vascularized organs. One notable limitation in our demonstration involves a lack of circulatory perfusion system similar to mammalian vascular networks. Nevertheless, we have demonstrated the practicality of this novel culture system and can be further improved through looped pumping of culture media using an intravenous cord to ensure organ-to-organ crosstalk is thorough. Though unlimited by cell type and chamber size, our biomimetic leaf chip only performs half-and-half experimental conditions. Thus, consideration is required when performing multi-organ studies to ensure successful perfusion culture of various organoids. Further development of our system is envisioned to provide a better tool for the tissue engineering field for therapeutics proof-of-concept studies and insight into circulatory-related conditions such as metastasis.

Methods

Fabrication of the biomimetic vascular network in silicon wafer

The high-quality photo of the leaf venation skeleton with hierarchical bifurcating veins was acquired using a consumer CCD camera (Cannon ED560 with micro-lens), as previously

described.[26] Briefly, fresh Osmanthus Fragrans leaves were boiled in sodium hydroxide solution (10 wt.%) to remove the soft tissue, washed with distilled water and air-dried to acquire the flat leaf venation skeleton. The photo was then imported into the software, Leaf Extraction and Analysis Framework Graphical User Interface (LEAF GUI), to extract the framework of the leaf venation and obtain the binary image. Afterwards, the binary image was processed in the software of WinTopo to obtain the CAD file of the leaf venation network, which could be edited freely through the software of AutoCAD. In our experiment, the Y-shaped inlet, outlet and the chambers with different diameters were added into the leaf venation network. The edited CAD file could be used to fabricate a photo-mask for the subsequent photolithography. Silicon wafers with a 150 μm depth of leaf venation network integrated with chambers could be made via SU-8 micropatterning methods that were established and detailed in our previous works.[24] The microscopic profile of the chamber with the connected microfluidic network was observed with a laser confocal microscopy (Olympus OLS 4000, Japan).

Assembly of the biomimetic vascular system

To replicate the microvascular network of leaf venation into the PDMS layer, the silicon wafer was pre-treated with Octafluorocyclobutane (C_4F_8) in an inductively coupled plasma (ICP) etching machine (Oxford, ICP180) for 5 minutes to facilitate subsequent demolding. PDMS prepolymer solution (Sylgard 184; Dow Corning, MI, USA) was uniformly mixed with curing agents with a mass ratio of 10:1, degassed in a vacuum chamber and finally cast onto pre-treated silicon mold. The PDMS layer with a negative pattern of leaf venation was peeled off after solidification at 95℃ for 2 hours, soaked in ethyl alcohol (75%) for 12 hours to clean the remaining C_4F_8, washed with ultrapure water and trimmed to obtain the finial PDMS layer with

the biomimetic vascular network. The inlet and outlet holes were punched using a 23G needle. The upper PMMA layers with a 1.5mm diameter hole and bottom layers with no hole were machined as designed. Afterwards, the PDMS layer was sandwiched by two PMMA slides and compressed together by ten screws and nuts. The inlet was connected to a 1 mL plastic syringe with a 23G needle using tubing with an inner diameter of 0.6 mm. The assembled leaf microfluidic chip was perfused with red dye solution and visualized with optical microscopy (Nikon, Ti-5) to characterize the connection of chambers and the biomimetic microfluidic network. A panoramic photo was captured using a consumer camera.

Perfusion experiment within the biomimetic vascular system

To characterize the half-and-half perfusion within the biomimetic vascular system, pure water and dyes were perfused, which process was recorded using a consumer camera. Before the dye perfusion experiments, the chips were immersed in water and then vacuumed to remove all the bubbles in seconds. Firstly, water and blue dye were perfused in the chip with no chamber through the two openings of the Y-shaped inlet respectively. When the blue dye suffused half of the chip, the water was replaced by red dye for perfusion. The representative images of dye perfusion were extracted every 3 seconds, which were imported into the ImageJ software (http://rsbweb.nih.gov/ij/) to calculate the perfused area. To study the flow transfer within the chips with integrated chambers, 1.5 mL 3 mg/mL fibrin hydrogel was filled in the chambers of the PDMS layer, which was then sandwiched by two PMMA slides and assembled. The biomimetic vascular system filled with fibrin hydrogel could also be vacuumed to suffuse water and perfused with dyes as previously.

Modeling and flow analysis of flow transfer within the biomimetic vascular system

Modeling and fluid dynamics analysis within the biomimetic vascular system was carried out as previously described in detail.[26] Briefly, the photo of leaf venation networks was processed by the software of LEAF GUI, WinTopo, AutoCAD and Gambit successively to obtain MESH file of leaf venation, which was finally imported into the ANSYS Fluent software to simulate the fluid flow inside the microfluidic channels and chambers of biomimetic vascular systems. Since the chambers will be added with 3D hydrogel for the perfusion experiments, the chambers are considered as the porous zones to simulate the 3D hydrogel material.

The CaseMapDiff Calculator is a function of the software Ansys Ensight, to compare a variable across different cases. The cases of fluid dynamics analysis within biomimetic vascular systems with 0 and 6 chambers processed by ANSYS Fluent were imported into Ansys Ensight and processed using the CasemapDiff Calculator function to generate the velocity difference between them.

FITC-dextran diffusion study within the biomimetic vascular system

To assess nutrition supply within the chamber filled with 3D fibrin hydrogel, solutions containing 200 mg/mL FITC-dextran (70 kDa, Sigma-Aldrich) were introduced, and fluorescence images were captured using a fluorescence microscope (Nikon, TI-E ECLIPSE) after 20 min, 40 min and 60 min of perfusion. To quantitatively characterize the mass transport within the chambers, the fluorescence image was loaded into ImageJ software and straight lines were drawn as the measurement baselines. The fluorescent intensity along the measurement baseline was analyzed and calculated by subtracting the fluorescence intensity of the dark background. Finally, we quantified the average fluorescence intensity of the chambers in the

different positions using ImageJ software.

Cell culture

Primary HUVECs (Angio-Proteomie) were cultured in endothelial growth medium (EGM-2MV; Lonza). Mouse bone marrow mesenchymal stem cells (mBMSCs, Cyagen) were cultured in Minimum Essential Medium α (MEM α, Thermo Fisher) supplemented with 10% fetal bovine serum (FBS, Gibco) and 1% penicillin/streptomycin (PS, Life Technologies). The human liver cancer cell line HepG2, a gift of Dr. Youhua Tan (Department of Biomedical Engineering, The Hong Kong Polytechnic University) and the human pancreatic cancer cell line PANC-1, kindly provided by Stem Cell Bank, Chinese Academy of Sciences were maintained in Dulbecco's Modified Eagle's Medium (DMEM, Thermo Fisher) supplemented with 10% fetal bovine serum (FBS, Gibco) and 1% penicillin/streptomycin (PS, Life Technologies). All the experiments were conducted using HUVECs of passage 6 or lower and mBMSCs of passage 10 or lower. The cells were labeled by green, red and violet color using Cell Tracker Green CMFDA Dye (C7025, Thermo Fisher), Red CMTPX Dye (C34552, Thermo Fisher) and CellTracker™ Violet BMQC Dye (C10094, Thermo Fisher) respectively.

Formation of 3D branched microvascular network within chambers

Before cell seeding, fibrinogen (6 mg/mL and 1 mg/mL) from bovine plasma (Sigma-Aldrich) and thrombin (100 U/mL) from bovine plasma (Sigma-Aldrich) were separately dissolved in PBS. 100 U/mL thrombin was mixed with EGM-2 MV (Lonza) to obtain a 6 U/mL thrombin solution for crosslinking fibrinogen. To enhance the attachment of HUVECs within the channels, the autoclaved PDMS layer with biomimetic vascular networks was covered by 1 mg/mL

fibrinogen solution for 1 hour in an incubator. Afterwards, the remaining fibrinogen solution was removed and the PDMS layer was placed in an incubator overnight to restore its hydrophobicity.

Primary HUVECs were detached and spun down at 200 g for 5 minutes and the cell pellet was resuspended in the prepared thrombin solution at 1×10^7/mL. The cell suspension was mixed with 6 mg/mL fibrinogen at a 1:1 volume ratio, quickly pipetted into the PDMS layer with 1.5 μL in each chamber and then placed in an incubator to polymerize for 10 minutes. The final concentration of HUVECs was 0.5×10^7/mL in 3 mg/mL fibrin gel. Two PMMA sheets, sterilized using UV light, were then used to sandwich the PDMS layer and assembled into the final chip. EGM-2 medium was then introduced by a syringe for subsequent dynamic culture at 20 μL/min. Cell viability of the self-assembled 3D branched microvascular network was characterized with a live/dead viability kit (L3224, Invitrogen). The living cells were stained with green color while the dead cells were stained with red color. F-actin/nuclei staining was further performed for the constructs cultured for 3 days. To characterize the growth of microvasculature within different chambers, confocal images of F-acting staining were analyzed using ImageJ software. Briefly, raw images were prepared by enhancing contrast and removing noise. An automatic threshold was used to produce binarized images. From 2D projections, the vessel area within each chamber was computed by ImageJ.

Endothelialization of the biomimetic vascular networks to connect the self-assembled 3D vasculature in the chambers

Primary HUVECs, labeled with green cell tracker, were encapsulated in 3 mg/mL fibrin gel and seeded into the chambers according to the procedure above. The assembled chips were then fully perfused by the fresh medium for half an hour to avoid any bubble inside the microfluidic

channels. 2×10^7/mL HUVEC suspension, labeled with red cell tracker, was injected into the empty microfluidic channels and incubated for 1 hour. Afterwards, we flipped over the chips and introduced the HUVEC suspension at 2×10^7/mL again in order to seed cells to all the inner surfaces of the empty channels. EGM-2 medium was then continuously perfused at 20 μL/min to favor cell adhesion and spreading. The fluorescence images were taken by using the laser confocal microscopy at 10X and invert microscopy (Nikon, Ti-5) at 4X. The 4X images were stitched together to obtain a panoramic image of the green self-assembled vasculature in chambers which were connected by the red endothelialized biomimetic vascular networks.

Organ-specific pancreatic cancer metastasis study within the biomimetic vascular system

To differentiate the various types of cells for studying pancreatic cancer metastasis into the vascularized organs in the biomimetic vascular system, primary HUVECs were labeled with green cell tracker, HepG2 cells and MSCs were labeled with violet cell tracker, and PANC-1 cells were labeled with red cell tracker. A cell suspension of HUVECs of 0.5×10^7/mL and HepG2 cells of 2.5×10^6/mL in 3 mg/mL fibrin gel was seeded into the chambers (1.5 μL cell suspension in each chamber) within half of the biomimetic vascular system to generate vascularized liver organs, while a cell suspension of HUVECs of 0.5×10^7/mL and MSCs of 1.25×10^6/mL in 3 mg/mL fibrin gel was seeded into the chambers (1.5 μL cell suspension in each chamber) within another half of the biomimetic vascular system to generate vascularized bone organs. MSCs were seeded at half of the cell density applied for HepG2 cells because of their higher proliferation rate, which could lead to overpopulation and microvasculature disruption. The mixed medium of 50% EGM-2 medium and 50% DMEM was used to perfuse the liver organs, while the mixed medium of 50% EGM-2 medium and 50% MEM α was used to perfuse the bone organs at 20

μL/min.

After 4 days in perfusion culture, PANC-1 cells was seeded by infusing 0.5mL of 2×10^6 cell suspension into the chip. The occupation of PANC-1 cells within vascularized organs was observed using a confocal fluorescence microscope (Leica 6000) after 6 days in perfusion culture. The red cancer cell number was counted from confocal imaging.

Statistical analysis

All quantitative results were presented as mean ± standard deviation. Statistical significance was determined using one-way statistical analysis of variance (ANOVA) followed by Tukey post-hoc test for multiple comparisons using SPSS statistical software. The differences were considered statistically significant if the value of p was <0.05 (*), $p < 0.01$(**).

Supporting Information

Supporting Information is available from the Wiley Online Library or from the author.

Acknowledgments

This work was financially supported by the General Research Fund (15202119) and Germany/HK Joint Research Scheme (G-PolyU508/18) from the Hong Kong Research Grants Council, Intra-faculty fund (ZVPC) from the Hong Kong Polytechnic University, Open fund from the Guangdong Provincial Key Laboratory of Functional Soft Condensed Matter, National Key R&D Program of China (2016YFC1101302, 2018YFA0703000), General Program (31871016, 51675412, 51422508) and the National Key Scientific Instrument and Equipment Development Projects (61827806) from the National Natural Science Foundation of China, the

Key Research Project of Shaanxi Province (2017ZDXM-GY-058), the Youth Innovation Team of Shaanxi Universities and the Fundamental Research Funds for the Central Universities.

Mao Mao and Ho Pan Bei contributed equally to this work.

Received: ((will be filled in by the editorial staff))
Revised: ((will be filled in by the editorial staff))
Published online: ((will be filled in by the editorial staff))

References

1. Chen, M. B.; Whisler, J. A.; Fröse, J.; Yu, C.; Shin, Y.; Kamm, R. D., *Nature Protocols* **2017,** *12*, 865. DOI 10.1038/nprot.2017.018 https://www.nature.com/articles/nprot.2017.018#supplementary-information.
2. Jeon, J. S.; Bersini, S.; Gilardi, M.; Dubini, G.; Charest, J. L.; Moretti, M.; Kamm, R. D., *Proceedings of the National Academy of Sciences* **2015,** *112* (1), 214. DOI 10.1073/pnas.1417115112.
3. Zheng, Y.; Chen, J.; Craven, M.; Choi, N. W.; Totorica, S.; Diaz-Santana, A.; Kermani, P.; Hempstead, B.; Fischbach-Teschl, C.; López, J. A.; Stroock, A. D., *Proceedings of the National Academy of Sciences* **2012,** *109* (24), 9342-9347. DOI 10.1073/pnas.1201240109.
4. Yildirimer, L.; Zhang, Q.; Kuang, S.; Cheung, C.-W. J.; Chu, K. A.; He, Y.; Yang, M.; Zhao, X., *Biofabrication* **2019,** *11* (3), 032003.
5. Huang, G.; Li, F.; Zhao, X.; Ma, Y.; Li, Y.; Lin, M.; Jin, G.; Lu, T. J.; Genin, G. M.; Xu, F., *Chemical reviews* **2017,** *117* (20), 12764-12850.
6. Qiu, Y.; Ahn, B.; Sakurai, Y.; Hansen, C. E.; Tran, R.; Mimche, P. N.; Mannino, R. G.; Ciciliano, J. C.; Lamb, T. J.; Joiner, C. H.; Ofori-Acquah, S. F.; Lam, W. A., *Nature Biomedical Engineering* **2018,** *2* (6), 453-463. DOI 10.1038/s41551-018-0224-z.
7. Zervantonakis, I. K.; Hughes-Alford, S. K.; Charest, J. L.; Condeelis, J. S.; Gertler, F. B.; Kamm, R. D., *Proc. Natl. Acad. Sci. U.S.A.* **2012,** *109* (34), 13515-13520. DOI 10.1073/pnas.1210182109.
8. Hasan, A.; Paul, A.; Vrana, N. E.; Zhao, X.; Memic, A.; Hwang, Y.-S.; Dokmeci, M. R.; Khademhosseini, A., *Biomaterials* **2014,** *35* (26), 7308-7325.
9. Bischel, L. L.; Young, E. W. K.; Mader, B. R.; Beebe, D. J., *Biomaterials* **2013,** *34* (5), 1471-1477. DOI https://doi.org/10.1016/j.biomaterials.2012.11.005.
10. Kolesky, D. B.; Truby, R. L.; Gladman, A. S.; Busbee, T. A.; Homan, K. A.; Lewis, J. A., *Adv. Mater.* **2014,** *26* (19), 3124.
11. Wong, K. H. K.; Truslow, J. G.; Khankhel, A. H.; Chan, K. L. S.; Tien, J., *Journal of Biomedical Materials Research Part A* **2013,** *101A* (8), 2181-2190. DOI 10.1002/jbm.a.34524.
12. Lee, V. K.; Kim, D. Y.; Ngo, H.; Lee, Y.; Seo, L.; Yoo, S.-S.; Vincent, P. A.; Dai, G., *Biomaterials* **2014,** *35* (28), 8092-8102. DOI https://doi.org/10.1016/j.biomaterials.2014.05.083.
13. Zhang, B.; Montgomery, M.; Chamberlain, M. D.; Ogawa, S.; Korolj, A.; Pahnke, A.; Wells, L. A.; Massé, S.; Kim, J.; Reis, L., *Nature Materials* **2016,** *15* (6), 669.
14. Zheng, Y.; Chen, J.; López, J. A., *Nature Communications* **2015,** *6* (1), 7858. DOI

10.1038/ncomms8858.
15. Lee, H. J.; Diaz, M. F.; Price, K. M.; Ozuna, J. A.; Zhang, S.; Sevick-Muraca, E. M.; Hagan, J. P.; Wenzel, P. L., *Nature Communications* **2017,** *8* (1), 14122. DOI 10.1038/ncomms14122.
16. Li, J.; Wei, J.; Liu, Y.; Liu, B.; Liu, T.; Jiang, Y.; Ding, L.; Liu, C., *Lab on a Chip* **2017,** *17* (22), 3921-3933. DOI 10.1039/C7LC00343A.
17. Saias, L.; Autebert, J.; Malaquin, L.; Viovy, J.-L., *Lab on a Chip* **2011,** *11* (5), 822-832. DOI 10.1039/C0LC00304B.
18. *Tissue Engineering Part A* **2010,** *16* (5), 1469-1477. DOI 10.1089/ten.tea.2009.0118.
19. Barber, R. W.; Emerson, D. R., *Microfluid. Nanofluid.* **2008,** *4* (3), 179-191. DOI 10.1007/s10404-007-0163-6.
20. McCulloh, K. A.; Sperry, J. S.; Adler, F. R., *Nature* **2003,** *421* (6926), 939-42.
21. Wu, W.; Hansen, C. J.; Aragón, A. M.; Geubelle, P. H.; White, S. R.; Lewis, J. A., *Soft Matter* **2010,** *6* (4), 739-742. DOI 10.1039/B918436H.
22. Wu, W.; Guijt, R. M.; Silina, Y. E.; Koch, M.; Manz, A., *RSC Advances* **2016,** *6* (27), 22469-22475. DOI 10.1039/C5RA25890A.
23. Miali, M. E.; Colasuonno, M.; Surdo, S.; Palomba, R.; Pereira, R.; Rondanina, E.; Diaspro, A.; Pascazio, G.; Decuzzi, P., *ACS Applied Materials & Interfaces* **2019,** *11* (35), 31627-31637. DOI 10.1021/acsami.9b09453.
24. He, J.; Mao, M.; Liu, Y.; Shao, J.; Jin, Z.; Li, D., *Advanced Healthcare Materials* **2013,** *2* (8), 1108-1113.
25. Sack, L.; Dietrich, E. M.; Streeter, C. M.; Sánchez-Gómez, D.; Holbrook, N. M., *Proceedings of the National Academy of Sciences* **2008,** *105* (5), 1567-1572. DOI 10.1073/pnas.0709333105.
26. Mao, M.; Jiankang, H.; Yongjie, L.; Xiao, L.; Tianjiao, L.; Wenxing, Z.; Dichen, L., *Biofabrication* **2018,** *10* (2), 025008.
27. Gershlak, J. R.; Hernandez, S.; Fontana, G.; Perreault, L. R.; Hansen, K. J.; Larson, S. A.; Binder, B. Y.; Dolivo, D. M.; Yang, T.; Dominko, T., *Biomaterials* **2017,** *125*, 13-22.
28. Hu, D.; Cai, D., *Phys. Rev. Lett.* **2013,** *111* (13), 138701. DOI 10.1103/PhysRevLett.111.138701.
29. Bohn, S.; Magnasco, M. O., *Phys. Rev. Lett.* **2007,** *98* (8), 088702. DOI 10.1103/PhysRevLett.98.088702.
30. He, J.; Mao, M.; Li, D.; Liu, Y.; Jin, Z., *仿生工程学报(英文版)* **2014,** *11* (1), 109-114.
31. Katifori, E.; Szöllősi, G. J.; Magnasco, M. O., *Phys. Rev. Lett.* **2010,** *104* (4), 048704. DOI 10.1103/PhysRevLett.104.048704.
32. Massagué, J.; Obenauf, A. C., *Nature* **2016,** *529* (7586), 298-306. DOI 10.1038/nature17038.
33. Urosevic, J.; Garcia-Albéniz, X.; Planet, E.; Real, S.; Céspedes, M. V.; Guiu, M.; Fernandez, E.; Bellmunt, A.; Gawrzak, S.; Pavlovic, M.; Mangues, R.; Dolado, I.; Barriga, F. M.; Nadal, C.; Kemeny, N.; Batlle, E.; Nebreda, A. R.; Gomis, R. R., *Nat. Cell Biol.* **2014,** *16* (7), 685-694. DOI 10.1038/ncb2977.
34. Obenauf, A. C.; Massagué, J., *Trends in Cancer* **2015,** *1* (1), 76-91. DOI https://doi.org/10.1016/j.trecan.2015.07.009.
35. Caballero, D.; Kaushik, S.; Correlo, V. M.; Oliveira, J. M.; Reis, R. L.; Kundu, S. C., *Biomaterials* **2017,** *149*, 98-115. DOI https://doi.org/10.1016/j.biomaterials.2017.10.005.
36. Saito, K.; Sakaguchi, M.; Maruyama, S.; Iioka, H.; Putranto, E. W.; Sumardika, I. W.;

Tomonobu, N.; Kawasaki, T.; Homma, K.; Kondo, E., *Journal of Cancer* **2018,** *9* (16), 2916-2929. DOI 10.7150/jca.24415.
37. Beckermann, B. M.; Kallifatidis, G.; Groth, A.; Frommhold, D.; Apel, A.; Mattern, J.; Salnikov, A. V.; Moldenhauer, G.; Wagner, W.; Diehlmann, A.; Saffrich, R.; Schubert, M.; Ho, A. D.; Giese, N.; Büchler, M. W.; Friess, H.; Büchler, P.; Herr, I., *Br. J. Cancer* **2008,** *99* (4), 622-631. DOI 10.1038/sj.bjc.6604508.